Journal Pre-proof

Method for generating right ventricular pressure–volume loops in routine practiceRV PV loop method for routine practice

Nils Kremer, Felix Glocker, Simon Schaefer, Patrick Janetzko, Athiththan Yogeswaran, Zvonimir Rako, Bruno Thal, Hans-Bernd Hopf, Werner Seeger, Hossein-Ardeschir Ghofrani, Paul M Heerdt, Khodr Tello

PII: S1053-2498(25)02256-9

DOI: https://doi.org/10.1016/j.healun.2025.09.002

Reference: HEALUN8609

To appear in: *Journal of Heart and Lung Transplantation*

Received date: 4 June 2025
Revised date: 24 August 2025
Accepted date: 2 September 2025

Please cite this article as: Nils Kremer, Felix Glocker, Simon Schaefer, Patrick Janetzko, Athiththan Yogeswaran, Zvonimir Rako, Bruno Thal, Hans-Bernd Hopf, Werner Seeger, Hossein-Ardeschir Ghofrani, Paul M Heerdt and Khodr Tello, Method for generating right ventricular pressure–volume loops in routine practiceRV PV loop method for routine practice, *Journal of Heart and Lung Transplantation,* (2025) doi:https://doi.org/10.1016/j.healun.2025.09.002

Method for generating right ventricular pressure–volume loops in routine practice

Running title: RV PV loop method for routine practice

Nils Kremer, MD,[a]* Felix Glocker, MSc,[a]* Simon Schaefer,[a] Patrick Janetzko,[a] Athiththan Yogeswaran, MD,[a] Zvonimir Rako, MD,[a] Bruno Thal,[a] Hans-Bernd Hopf, MD,[b] Werner Seeger, MD,[a,c] Hossein-Ardeschir Ghofrani, MD,[a] Paul M Heerdt, MD PhD,[d]* Khodr Tello, MD[a]*

From the [a]Department of Internal Medicine, Justus-Liebig-University Giessen, Universities of Giessen and Marburg Lung Center, Member of the German Center for Lung Research, Giessen, Germany; [b]Department of Anaesthesia, Perioperative Medicine and Interdisciplinary Intensive Care Medicine, Asklepios Klinik Langen, Langen, Germany; [c]Institute for Lung Health (ILH), Giessen, Germany; and the [d]Department of Anesthesiology, Yale University School of Medicine, New Haven, CT.

*Authors contributed equally.

Corresponding author: Khodr Tello, MD, Department of Internal Medicine, Justus-Liebig-University Giessen, Klinikstrasse 32, 35392 Giessen, Germany. Telephone: +49 (0)641 985 56087. Fax: +49 (0)641 985 42599. Email: khodr.tello@innere.med.uni-giessen.de.

Twitter handles

NK: @nilskremermd.bsky.social

KT: @khodrtello.bsky.social

Tweet: PV loop analysis is the gold standard for RV function, but conductance cath limits clinical use. New method reconstructs RV PV loops from Swan-Ganz pressures, matching conductance cath & 3D echo for broader adoption.

Manuscript word count: 3587

Abstract word count: 250

Non-standard abbreviations in main text

CTEPH, chronic thromboembolic pulmonary hypertension

Ea, arterial elastance

EDV, end-diastolic volume

Ees, end-systolic elastance

EF, ejection fraction

ESP, end-systolic pressure

ESV, end-systolic volume

IpcPH, isolated postcapillary pulmonary hypertension

PAH, pulmonary arterial hypertension

P_{max}, theoretical peak pressure under isovolumic conditions

PV, pressure–volume

SV, stroke volume

SW, stroke work

uEDV, uncalibrated end-diastolic volume

uSV, uncalibrated SV

Abstract

Background: Analysis of pressure–volume (PV) loops from conductance catheterization is the gold standard for evaluating right ventricular (RV) function, but the complexity of conductance

catheterization limits clinical implementation. This study validates a novel method for reconstructing RV PV loops from pressure waveforms acquired during routine right heart catheterization (RHC).

Methods: An algorithm was developed to estimate RV volume from pressure using the hydromotive source pressure model with external calibration. The method was validated against conductance catheterization in swine (preclinical cohort) and in patients with pulmonary hypertension (clinical cohort), and against 3-dimensional echocardiography in patients with routine RHC (feasibility cohort). Agreement was assessed using Bland–Altman analysis and correlation.

Results: In the preclinical cohort (n = 10, 22 recordings), pressure-derived stroke work (SW) demonstrated very good agreement with conductance values (bias –0.4%; percentage error 7.0%). End-diastolic volume (EDV) showed moderate agreement (bias 3.7%; percentage error 29.0%). In the clinical cohort (n = 44, 44 recordings), agreement was good for SW (bias –2.8%; percentage error 14.6%), and borderline for EDV (bias –5.5%; percentage error 35.3%). In the feasibility cohort (n = 29, 29 recordings), agreement was good for ejection fraction (bias 2.2%, percentage error 30.3%) and moderate for stroke volume, EDV, end-systolic elastance, and arterial elastance. All parameters correlated strongly with reference values (Pearson $r \geq 0.79$, $p < 0.001$).

Conclusion: This pressure-based method reconstructs RV PV loops from standard RHC data and reliably estimates SW, contractility, and afterload, supporting its integration into routine clinical workflows (tool freely available at https://pv-loop-generator.onrender.com).

Keywords: pressure–volume loop, right heart catheterization, conductance catheter, right ventricular function, hemodynamics

Introduction

Pressure–volume (PV) loop analysis is widely regarded as the gold standard for characterizing right ventricular (RV) function in both health and disease [1,2]. The simultaneous acquisition of RV pressure and volume enables time-resolved assessment of ventricular mechanics, including end-diastolic and end-systolic PV relationships. From these loops, key parameters such as end-systolic elastance (Ees),

effective arterial elastance (Ea), and their ratio (Ees/Ea) can be derived to quantify RV–pulmonary arterial coupling [1]. This coupling index reflects the ability of the right ventricle to adapt its contractility to changes in afterload and is a central determinant of cardiac output, symptom burden, exercise capacity, and long-term prognosis [5,10,11].

The clinical relevance of RV PV loop-derived metrics continues to grow across various cardiovascular conditions, including pulmonary hypertension [3-6], heart failure with preserved ejection fraction (EF) [7], valvular heart disease [8], and mechanical circulatory support [9]. In particular, impaired RV–pulmonary arterial coupling has emerged as a strong prognostic marker in advanced disease states. For instance, in patients undergoing transcatheter tricuspid valve interventions, Ees/Ea has been shown to outperform traditional echocardiographic markers such as tricuspid annular plane systolic excursion in predicting outcomes [23]. Similarly, in patients with RV failure following left ventricular assist device implantation, reduced coupling correlates with increased morbidity and mortality [24].

Currently, the conductance catheter remains the gold standard for simultaneous measurement of RV pressure and volume [1]. This system incorporates a pressure transducer and multiple sensing electrodes to estimate instantaneous volume based on blood conductance [1]. However, the technique is highly invasive and technically demanding, often requiring wire and imaging guidance to navigate the right ventricle and achieve stable positioning. Misalignment, contact artifacts, and segmental displacement can lead to inaccurate measurements. These practical challenges, combined with high equipment cost and limited availability, restrict the use of conductance catheterization to specialized research settings. While noninvasive surrogates from echocardiography and magnetic resonance imaging (MRI) offer prognostic value [12, 13] their moderate correlation with RV PV loop metrics and inability to differentiate key components like Ees and Ea limit their effectiveness [14].

To address these limitations, we developed and validated a simplified method for RV PV loop reconstruction using standard pressure catheters, specifically the Swan–Ganz catheter, combined with a computational model that estimates volume curves from pressure waveforms. Based on the hydromotive source pressure model [15, 16] and calibrated externally, the algorithm enables real-time derivation of RV PV loops and coupling metrics without the need for specialized volumetric

instrumentation. This approach significantly lowers the technical barrier to RV PV analysis and has the potential to enable widespread clinical adoption of advanced RV hemodynamic assessment in both routine and interventional settings.

Methods

Study design

The study was conducted in three sequential phases: preclinical, clinical validation, and feasibility testing. These phases were designed to comprehensively assess the accuracy, robustness, and clinical applicability of the pressure-only algorithm for RV PV loop reconstruction. Preclinical experiments were conducted under optimal laboratory conditions in accordance with Institutional Animal Care and Use Committee approved protocols. Clinical studies conformed with the principles of the Declaration of Helsinki and were approved by the Ethics Committee of the University of Giessen (Approval no. 266/11 & 108/15). All participating patients provided written informed consent.

Preclinical validation

In the preclinical phase, RV pressure and volume data were acquired from 10 anesthetized swine using 5F conductance catheters (12 electrodes, 7 mm spacing; Millar Instruments, Houston, TX) inserted via median sternotomy. Parallel conductance was corrected by hypertonic saline injection, and stroke volume (SV) was calibrated using an ascending aortic ultrasonic flow probe. Signals were recorded with a sample rate of 200 Hz and SV was calculated as the difference between the volumes at the timepoints of $dpdt_{max}$ and $dpdt_{min}$.

Clinical validation

The clinical validation phase included 44 patients from the *Right-Heart I* study (NCT03403868), comprising 22 individuals with Group 1 pulmonary arterial hypertension (PAH) or Group 4 chronic thromboembolic pulmonary hypertension (CTEPH), 7 with isolated postcapillary pulmonary hypertension (IpcPH), and 15 controls. All participants underwent right heart catheterization with simultaneous conductance catheterization to acquire RV pressure and volume data. Volumetric calibration was performed via cardiac MRI, typically conducted within a clinically acceptable time window (<24 h). Conductance catheter measurements were selected based on the quality of the pressure

and volume waveforms, as well as variability in hemodynamic conditions, in order to represent a broad spectrum of PV loop morphologies across a wide range of RV functional states. Signals were recorded with a sample rate of 250 Hz and SV was calculated as the difference between the volumes at the timepoints of $dpdt_{max}$ and $dpdt_{min}$.

Feasibility testing

To evaluate the clinical feasibility of pressure-only RV PV loop generation using standard equipment, the algorithm was applied to RV pressure waveforms obtained from 29 patients undergoing routine right heart catheterization for clinical reasons at the University Hospital of Giessen. All procedures were performed using a 7.5 F Swan–Ganz VIP+ catheter (Edwards Lifesciences, Irvine, CA, USA), which includes a dedicated lumen for high-fidelity RV pressure measurement. Pressure signals were digitally recorded at 250 Hz and exported from the GE Mac-Lab hemodynamic system (GE Medical Systems, Milwaukee, WI, USA) for offline analysis. Calibration was performed using thermodilution-based cardiac output, and the resulting RV PV loop-derived metrics were compared with reference values obtained from 3-dimensional (3D) transthoracic echocardiography conducted within a standardized clinical timeframe of less than 24 h (Philips Epiq 7G, Philips Healthcare, Best, the Netherlands). SV was calculated as the ratio between cardiac output from thermodilution and the heart rate.

Signal processing and RV PV loop generation

The algorithm reconstructs RV PV loops from pressure waveforms using a stepwise approach (Figure 1 and supplemental methods). We use the term 'pressure-only' to differentiate the algorithm from conductance catheter methods, which measure both pressure and volume signals using physical sensors, although external SV calibration is required for full implementation. The process begins with the identification of key inflection points on the pressure trace: the maximal and minimal derivatives of pressure $dpdt_{max}$ and $dpdt_{min}$. Tangents are drawn at these points, and their intersection is used to estimate the isovolumic pressure P_{max} [17], which represents the theoretical peak pressure the ventricle would generate under isovolumic conditions.

Next, a hydromotive source pressure waveform [15, 16] is constructed by connecting the key pressure landmarks—$dpdt_{max}$, P_{max}, and $dpdt_{min}$—using cubic spline interpolation, constrained by the respective

pressure derivatives at the boundaries. The resulting waveform approximates the idealized driving pressure responsible for ventricular ejection [16].

Systolic flow is estimated by subtracting the measured RV pressure from the hydromotive pressure curve. The resulting pressure gradient is assumed to be proportional to instantaneous flow, which is then numerically integrated over time to derive an uncalibrated volume waveform. The diastolic portion of the volume curve is completed by interpolating between the uncalibrated end-systolic volume (ESV) and end-diastolic volume (EDV, Figure 1).

End-systolic pressure (ESP) is determined by identifying the point of maximal elastance, defined as the time point with the highest ratio of pressure to uncalibrated volume. This approach avoids reliance on indirect approximations and supports physiologically grounded assessment of contractility [18].

In the final calibration step, uncalibrated SV and EF are scaled using external reference values obtained from thermodilution or 3D echocardiography. Calibrated EDV is then computed as SV divided by EF. For applications where external calibration is not available, EF can also be estimated directly from the pressure waveform using the empirical relationship $EF = 1 - (ESP/P_{max})$ [19, 20].

The complete algorithm is implemented as a web-based tool, freely available at https://pv-loop-generator.onrender.com.

All signals were low-pass filtered at 10 Hz to suppress high-frequency noise. To compensate for the resulting attenuation of waveform derivatives, a scaling factor of 1.2 was applied to both $dpdt_{max}$ and $dpdt_{min}$ prior to their use in the algorithm. All available beats (usually between 5 and 20 per sample) were interpolated to the mean beat length and averaged by summing corresponding values and dividing by the total number of beats. Variables were then extracted from the averaged PV loops obtained using both the pressure-only method and the reference conductance catheter data [26].

In summary, the algorithm consists of the following steps:

- Estimate the P_{max} curve and ESP from the RV pressure waveform.
- Compute the uncalibrated outflow curve as the difference between the P_{max} curve and the RV pressure curve and calculate uncalibrated SV (uSV) as the integral.

- Estimate EF using the relationship EF = 1 − ESP/P_{max} and uncalibrated EDV as uEDV = uSV/EF.
- Integrate the outflow curve to construct the systolic portion of the volume curve and generate the diastolic portion of the volume curve by fitting a spline between uESV and uEDV.
- Combine the systolic and diastolic segments to form the complete uncalibrated volume curve.
- Calibrate the volume curve using externally measured SV, obtained from thermodilution, 3D echocardiography, or cardiac MRI.

Calibration of conductance catheters

The conductance signal C(t) from a conductance catheter reflects RV volume over time and requires calibration using a gain factor α and an offset factor Vp to yield absolute volume measurements. Calibration techniques vary, with α typically derived from SV comparisons and Vp estimated either through hypertonic saline injection or imaging-based methods like MRI, both of which are sensitive to catheter position and segmentation, necessitating recalibration if the catheter is repositioned [1].

Outcome measures

To evaluate the validity of the pressure-derived RV PV loops, seven key outcome measures were assessed: EF, SV, EDV, ESV, stroke work (SW), Ees, and Ea. These variables were selected to characterize both global systolic function and the interaction between the right ventricle and the pulmonary circulation.

EF and SV served as global indicators of systolic performance, while EDV was used to assess the accuracy of absolute volume scaling following external calibration. SW, defined as the area enclosed by the PV loop, quantified the mechanical work performed by the right ventricle during a single cardiac cycle. Ees, calculated as the difference between maximal pressure and ESP/SV, served as a load-independent index of myocardial contractility. Ea, defined as ESP/SV, quantified the effective afterload imposed by the pulmonary circulation. The ratio Ees/Ea was not evaluated, as the single-beat method for Ees/Ea relies solely on pressure measurements and would yield identical results regardless of the volume estimation method used.

In the preclinical and clinical validation cohorts, volume calibration was performed using conductance-derived SV, enabling independent assessment of EDV and SW. Since SV was used for calibration, direct comparisons of SV were constrained by calibration alignment. Accordingly, validation focused on EDV and SW—parameters that reflect the volume axis and loop area, respectively. SW was selected as the primary functional metric because it captures PV loop morphology independently of absolute volume scaling and, unlike other variables, incorporates the entire volume curve derived from pressure signals. For these reasons, SW is the most appropriate variable for validating the novel algorithm used to generate PV loops.

In the feasibility cohort, calibration was performed using thermodilution-derived SV, allowing for independent comparison of derived parameters, including EDV, ESV, SV, EF, Ees, and Ea, against reference values obtained from 3D echocardiography.

Statistical analysis

Data were assessed for normality using the Shapiro–Wilk test, with a p-value > 0.05 indicating a normal distribution. Normally distributed data were analyzed using unpaired t-tests for independent samples. Non-normally distributed independent samples were evaluated using the Mann–Whitney U test. Correlations between algorithm-derived parameters and reference values were assessed using the Pearson correlation coefficient; correlations between volumetric parameters derived from 3D echocardiography and those calculated from thermodilution and RV pressure waveforms were also assessed using Spearman's rank correlation coefficient. A p-value ≤ 0.05 was considered statistically significant. Normally distributed variables are reported as mean ± standard deviation, and non-normally distributed variables as median with interquartile range.

Agreement between measurement methods was evaluated using Bland–Altman analysis, and the degree of agreement was classified based on the percentage error, defined as 1.96 × standard deviation of the bias divided by the mean of the reference method. The interpretation framework was adapted from the commonly accepted standards established in the cardiac output validation literature [25], where a percentage error below 30% is generally considered acceptable for method interchangeability.

Results

Mean PV loops for the pressure-only and reference methods are shown in Figure 2.

Preclinical validation

In the preclinical cohort 22 individual measurements from 10 female Sinclair swine (age 6–122 months; size 35–120 kg) were recorded and algorithm-derived PV parameters were compared with reference data obtained from conductance catheters (Table 1 and Figure S1). The algorithm demonstrated very good agreement for SW, with a negligible mean bias of −0.4% and low percentage error (7.0%). Correlation was excellent (r = 1.00, $p < 0.001$). For EDV, agreement was moderate, with a bias of 3.7%, a percentage error of 29.0%, and correlation of r = 0.82 ($p < 0.001$). Thus, the results support the algorithm's ability to reliably quantify PV relations in a controlled preclinical setting.

Clinical validation

In the clinical cohort ($n = 44$; 27 female; Table 2), PV loop parameters derived from right heart catheter waveforms were validated against conductance catheter measurements. For SW, the algorithm showed good agreement, with a bias of −2.8% and a percentage error of 14.6%. Correlation remained strong (r = 0.99, $p < 0.001$; Table 1 and Figure S2). EDV also showed good correlation (r = 0.90, $p < 0.001$), but the agreement for EDV was moderate with a bias of −5.5% and a higher percentage error than SW (35.3%) (Table 1 and Figure S2).

To evaluate whether RV loading conditions affect the accuracy of the pressure-derived algorithm, we performed a *post hoc* subgroup analysis in the conductance cohort. Patients were split into low-ESP (21 ± 4 mm Hg, $n = 22$) and high-ESP (56.5 ± 11 mm Hg, $n = 22$) groups. Bland–Altman testing confirmed that SW remained accurate in both strata (percentage error 13.4% and 13.9%, respectively). EDV was less stable at higher load (bias −3.4% vs −7.6%; percentage error 29.0% vs 36.9%). Thus, the method preserves functional indices across pressure ranges, while volume estimates degrade modestly with rising RV afterload.

To determine whether diagnostic category influenced agreement, we also compared control, IpcPH, and PAH/CTEPH subgroups. Mean percentage bias for SW was −1.6 ± 8.0% in controls, −3.5 ± 7.0% in patients with IpcPH, and −3.5 ± 7.5% in those with PAH/CTEPH (analysis of variance

[ANOVA] $p = 0.75$; Kruskal–Wallis $p = 0.63$). Mean percentage EDV bias was $-10.1 \pm 27.9\%$, $6.8 \pm 35.4\%$, and $-9.0 \pm 18.0\%$, respectively (ANOVA $p = 0.29$; Kruskal–Wallis $p = 0.31$). Thus, agreement between methods is maintained independently of the underlying disease.

Feasibility testing

In the feasibility cohort of 29 patients (13 female; Table 3), PV loop analysis was performed using waveform data obtained from routine right heart catheterizations. Of the 29 individuals, 8 had no evidence of pulmonary hypertension, while the remaining 21 were diagnosed with pulmonary hypertension and classified according to clinical subtype: 10 in Group 1, 3 in Group 2, 4 in Group 3, 2 in Group 4, and 1 in Group 5.

Table 4 shows the comparison of volumetric and coupling parameters derived by the algorithm (calibrated by thermodilution) versus 3D echocardiography in the feasibility cohort. Bland–Altman analyses (Table 1 and Figures S3–S5) demonstrated good agreement for EF (bias = 2.2%, percentage error = 30.3%) and moderate agreement for EDV (bias = −4.4%, percentage error = 26.5%), SV (bias = −1.0%, percentage error = 30.2%), Ees (bias = −1.4%, percentage error = 34.8%), and Ea (bias = −1.4%, percentage error = 41.3%).

Discussion

This study presents and validates a novel method for generating RV PV loops using only pressure waveforms acquired during routine right heart catheterization. By reconstructing volume from the pressure signal via the hydromotive source pressure model and applying external calibration, the method circumvents the need for conductance catheterization or advanced volumetric imaging. Its compatibility with standard Swan–Ganz catheters underscore its practical feasibility in clinical workflows, addressing longstanding barriers to the broader adoption of RV PV loop analysis.

Across preclinical, clinical, and feasibility cohorts, the method consistently produced pressure-derived PV loops that aligned well with reference standards. In the preclinical cohort, comparison with conductance catheter measurements demonstrated very good agreement for SW, with negligible bias and low percentage error. EDV showed moderate agreement, reflecting expected variability in absolute volume estimation under experimental conditions.

In the clinical validation cohort, algorithm-derived SW maintained good agreement with conductance catheter reference values. However, EDV agreement was weaker. These findings suggest that while the method effectively reproduces the functional morphology of RV PV loops, absolute volume estimation may be less reliable in the presence of patient-specific anatomical variability or altered RV geometry. Moreover, in a clinical setting, calibration of conductance catheters is inherently less controlled than in preclinical models, further contributing to variability in absolute volume measurements and limiting the precision of volumetric validation. It should be emphasized that this limitation does not represent a disadvantage of the pressure-based method relative to conductance catheters, which also require calibration to known EDV and ESV values. When the pressure-based RV PV loop is calibrated against an independent volumetric reference, it produces accurate absolute volumes. Therefore, the observed EDV discrepancy pertains only to instances in which EDV is derived from pressure-based EF and SV.

Feasibility testing extended the validation to routine right heart catheterization workflows. In this setting, pressure-derived RV PV loop parameters calibrated by thermodilution were compared with measurements obtained from 3D echocardiography. Results demonstrated good agreement for EF and moderate agreement for EDV, SV, Ees, and Ea. All Spearman correlation coefficients exceeded 0.78, indicating strong monotonic relationships between the two modalities. Although the percentage error was variable across parameters, the magnitude and direction of biases remained within clinically acceptable ranges for most variables. These findings support the method's applicability for assessing global RV function and RV–pulmonary arterial coupling using data readily available in standard clinical practice.

Compared with existing alternatives, such as reconstruction from four empirically estimated corner points using cardiac MRI or 3D echocardiography-derived volumes, the proposed method offers the advantages of accurate presentation of loop shapes and direct identification of ESP at the point of maximal elastance, rather than relying on approximations based on waveform derivatives [21, 22]. This improves physiological accuracy and reduces dependence on supplementary imaging.

Nevertheless, several limitations should be acknowledged. First, the accuracy of the method is inherently linked to pressure signal quality. In fluid-filled systems, motion artifacts and damping can

distort waveform morphology. To mitigate this, we utilized Swan–Ganz catheters with a dedicated RV pressure lumen positioned proximally, allowing the distal tip to stabilize in the pulmonary artery and improving signal fidelity. Waveforms were digitized at 250 Hz to ensure adequate temporal resolution. To assess the impact of the recording method, we retrospectively analyzed 41 patients who underwent right heart catheterization with standard Swan–Ganz catheters, in which short RV waveform segments were recorded from the distal lumen during pullback from the pulmonary artery. Compared with a dedicated RV side port, distal recordings showed reduced accuracy for EDV while SV correlation was comparable (for details, see the supplemental results, Table S1, and Figure S6). These differences likely reflect the limited number of analyzable beats, the lower frequency response of the catheter tip, and frequent extrasystoles. Overall, the algorithm remained usable with distal tip tracings, though signal quality determined reliability: SV estimates were consistent, while EDV estimates showed broader limits of agreement. When distal signals met basic quality benchmarks, the method provided clinically meaningful results, with errors driven primarily by recording artifacts rather than the algorithm itself.

As a second limitation, the volume reconstruction assumes a zero unstressed volume (V_0) [19], which holds in non-dilated right ventricles but may introduce systematic bias in patients with RV dilation. This limitation manifested as a proportional bias in Bland–Altman comparisons of EF versus 3D echocardiography, although mean EF values remained consistent at the cohort level. This suggests that V_0 may be negligible at the population level, as supported by previous studies [17, 19]. Nonetheless, because V_0 can vary substantially, especially in markedly dilated or remodeled right ventricles, or in studies where serial changes in V_0 itself are of clinical interest, external calibration of EF (and thus EDV/ESV) remains necessary in these patients, just as with conductance-based methods.

Finally, the pressure-only method does not support segmental analysis of regional wall motion or dyssynchrony, which remains unique to conductance catheter systems. Although multi-beat preload-reduction protocols could theoretically be adapted, the current single-beat implementation favors practical scalability over complexity. Given the limited adoption of multi-beat protocols in clinical practice, the single-beat design aligns well with existing procedural workflows.

Conclusion

This study presents and validates a novel method for reconstructing RV PV loops using only pressure waveforms acquired during routine right heart catheterization. By applying a physiologically grounded computational model to the RV pressure signal, the approach eliminates the need for conductance catheterization or advanced volumetric imaging, thereby addressing longstanding limitations related to procedural complexity, cost, and limited accessibility.

The method is compatible with standard Swan–Ganz catheters, does not require advanced imaging guidance, and allows direct identification of ESP as the point of maximal elastance, avoiding reliance on indirect or empirical approximations. External calibration using thermodilution-derived SV enables clinical application without the need for MRI or 3D echocardiography in many settings.

By enabling advanced PV analysis using existing catheterization infrastructure, this method supports the integration of mechanistic RV assessment into standard diagnostic workflows. To promote clinical adoption and translational research, the computational algorithm has been made freely available as an open-access web tool (https://pv-loop-generator.onrender.com).

Acknowledgments

This work was funded by the Excellence Cluster Cardio-Pulmonary System and the Collaborative Research Center (SFB) 1213–Pulmonary Hypertension and Cor Pulmonale, grant number SFB1213/1, project B08 (German Research Foundation, Bonn, Germany).

Declaration of interests

Dr. Kremer has received speaker/consultancy fees from Janssen, AOP, OrphaCare and MSD outside the submitted work. F. Glocker is shareholder of emka medical and former chief operating officer of emka medical. Dr. Yogeswaran has received personal fees from MSD, AOP and OrphaCare outside the submitted work. Dr. Ghofrani has received fees for serving as a board member for AbbVie, Bellerophon Pulse Technologies, Medscape, OMT, UCB Celltech, and Web MD Global; consultancy fees and fees for serving on a steering committee for Actelion Pharmaceuticals, Bayer, Gilead Sciences, GlaxoSmithKline, Merck, Novartis, and Pfizer; lecture fees from Actelion Pharmaceuticals, Bayer,

GlaxoSmithKline, Merck, Novartis, and Pfizer; and grant support from Actelion Pharmaceuticals, Bayer, Novartis, and Pfizer. Dr. Seeger has received consultancy fees from Consultancy fees from Lung Biotechnology, Pieris Pharmaceuticals, Resyca BV, Tiakis and Thaerapy BV outside the submitted work. Dr. Hopf is chief medical officer and shareholder of emka medical. Dr. Heerdt reports general disclosures outside the submitted work to include consulting relationships with Edwards Lifesciences and Cardiage LLC and equity interest in emka Medical. Dr. Tello has received speaker/consultancy fees from Actelion, Janssen, Bayer, MSD, AOP and OrphaCare outside the submitted work. All other authors report no relationships that could be construed as a conflict of interest.

Data sharing

The data underlying this article cannot be shared publicly as they are part of ongoing projects and analyses within the Collaborative Research Center (SFP) 1213–Pulmonary Hypertension and Cor Pulmonale, grant number SFB1213/1, project B08 (German Research Foundation, Bonn, Germany). The data will be shared on reasonable request from the corresponding author.

References

1 Brener MI, Masoumi A, Ng VG, et al. Invasive Right Ventricular Pressure-Volume Analysis: Basic Principles, Clinical Applications, and Practical Recommendations. Circ Heart Fail 2022;15:e009101.

2 Rako ZA, Kremer N, Yogeswaran A, Richter MJ, Tello K. Adaptive versus maladaptive right ventricular remodelling. ESC Heart Fail 2023;10:762–75.

3 Tedford RJ, Mudd JO, Girgis RE, et al. Right Ventricular Dysfunction in Systemic Sclerosis–Associated Pulmonary Arterial Hypertension. Circ Heart Fail 2013;6:953–63.

4 Kremer N, Rako Z, Glocker F, Tello K. Monitoring of Right Ventricular Failure With Daily Pressure Volume Loops Obtained via an Application and 3-Dimensional Echocardiography. Circ Heart Fail 2023;16:e010097.

5 Yogeswaran A, Petermann R, Kremer NC, et al. Right ventricular – pulmonary arterial coupling predicts mortality in precapillary pulmonary hypertension. ERJ Open Res 2025;11:00685-2024.

6 Tello K, Kremer N, Richter MJ, et al. Inhaled Iloprost Improves Right Ventricular Load-Independent Contractility in Pulmonary Hypertension. Am J Respir Crit Care Med 2022;206:111-4.

7 Rommel K-P, von Roeder M, Oberueck C, et al. Load-Independent Systolic and Diastolic Right Ventricular Function in Heart Failure With Preserved Ejection Fraction as Assessed by Resting and Handgrip Exercise Pressure–Volume Loops. Circ Heart Fail 2018;11:e004121.

8 Sarraf M, Burkhoff D, Brener MI. First-in-Man 4-Chamber Pressure–Volume Analysis During Transcatheter Aortic Valve Replacement for Bicuspid Aortic Valve Disease. JACC Case Rep 2021;3:77-81.

9 Brener MI, Hamid NB, Fried JA, et al. Right Ventricular Pressure–Volume Analysis During Left Ventricular Assist Device Speed Optimization Studies: Insights Into Interventricular Interactions and Right Ventricular Failure. J Card Fail 2021;27:991–1001.

10 Tello K, Dalmer A, Axmann J, et al. Reserve of Right Ventricular-Arterial Coupling in the Setting of Chronic Overload. Circ Heart Fail 2019;12:e005512.

11 Kremer N, Schaefer S, Yogeswaran A, et al. Exercise Limitation in Pulmonary Hypertension – Physiological Insights into the Six-Minute Walk Test. Am J Respir Crit Care Med 2024;210:1486-90.

12 Tello K, Wan J, Dalmer A, et al. Validation of the Tricuspid Annular Plane Systolic Excursion/Systolic Pulmonary Artery Pressure Ratio for the Assessment of Right Ventricular-Arterial Coupling in Severe Pulmonary Hypertension. Circ Cardiovasc Imaging 2019;12:e009047.

13 Richter MJ, Peters D, Ghofrani HA, et al. Evaluation and Prognostic Relevance of Right Ventricular-Arterial Coupling in Pulmonary Hypertension. Am J Respir Crit Care Med 2020;201:116–9.

14 Golbin JM, Shukla N, Nero N, Hockstein MA, Tonelli AR, Siuba MT. Non-invasive surrogates for right Ventricular-Pulmonary arterial coupling: a systematic review and Meta-Analysis. Pulm Circ 2024;14:e70004.

15 Elzinga, G, Westerhof, N. End Diastolic Volume and Source Impedance of the Heart. In: Porter R, Fitzsimons DW, editors. Ciba Foundation Symposium 24 - Physiological Basis of Starling's Law of the Heart. Chichester, UK: John Wiley & Sons, Ltd; 1974. p. 241-55.

16 Sunagawa K, Yamada A, Senda Y, et al. Estimation of the hydromotive source pressure from ejecting beats of the left ventricle. IEEE Trans Biomed Eng 1980;27:299–305.

17 Kremer N, Glocker F, Schäfer S, et al. Precision cardiac monitoring: algorithmic real-time assessment of right ventricular function in pulmonary hypertension. ESC Heart Fail 2024;11:2469–72.

18 Singh I, Oakland H, Elassal A, Heerdt PM. Defining end-systolic pressure for single-beat estimation of right ventricle–pulmonary artery coupling: simple… but not really. ERJ Open Res 2021;7: 00219-2021.

19 Heerdt PM, Kheyfets V, Charania S, Elassal A, Singh I. A pressure-based single beat method for estimation of right ventricular ejection fraction: proof of concept. Eur Respir J 2020;55:1901635.

20 Heerdt PM, Singh I, Elassal A, Kheyfets V, Richter MJ, Tello K. Pressure-based estimation of right ventricular ejection fraction. ESC Heart Fail 2022;9:1436-43.

21 Vanderpool RR, Puri R, Osorio A, et al. Surfing the right ventricular pressure waveform: methods to assess global, systolic and diastolic RV function from a clinical right heart catheterization. Pulm Circ 2020;10:2045894019850993.

22 Tello K, Richter MJ, Axmann J, et al. More on Single-Beat Estimation of Right Ventriculoarterial Coupling in Pulmonary Arterial Hypertension. Am J Respir Crit Care Med 2018;198:816-8.

23 Brener MI, Lurz P, Hausleiter J, et al. Right Ventricular-Pulmonary Arterial Coupling and Afterload Reserve in Patients Undergoing Transcatheter Tricuspid Valve Repair. J Am Coll Cardiol 2022;79:448-61.

24 Scheel PJ III, Cubero Salazar IM, Friedman, et al. Occult right ventricular dysfunction and right ventricular-vascular uncoupling in left ventricular assist device recipients. J Heart Lung Transplant 2024;43:594-603.

25 Critchley LA, Critchley JA. A meta-analysis of studies using bias and precision statistics to compare cardiac output measurement techniques. J Clin Monit Comput 1999;15:85-91.

26 Stonko DP, Edwards J, Abdou H, et al. A technical and data analytic approach to pressure-volume loops over numerous cardiac cycles. *JVS Vasc Sci* 2022;3:73-84.

Figure legends

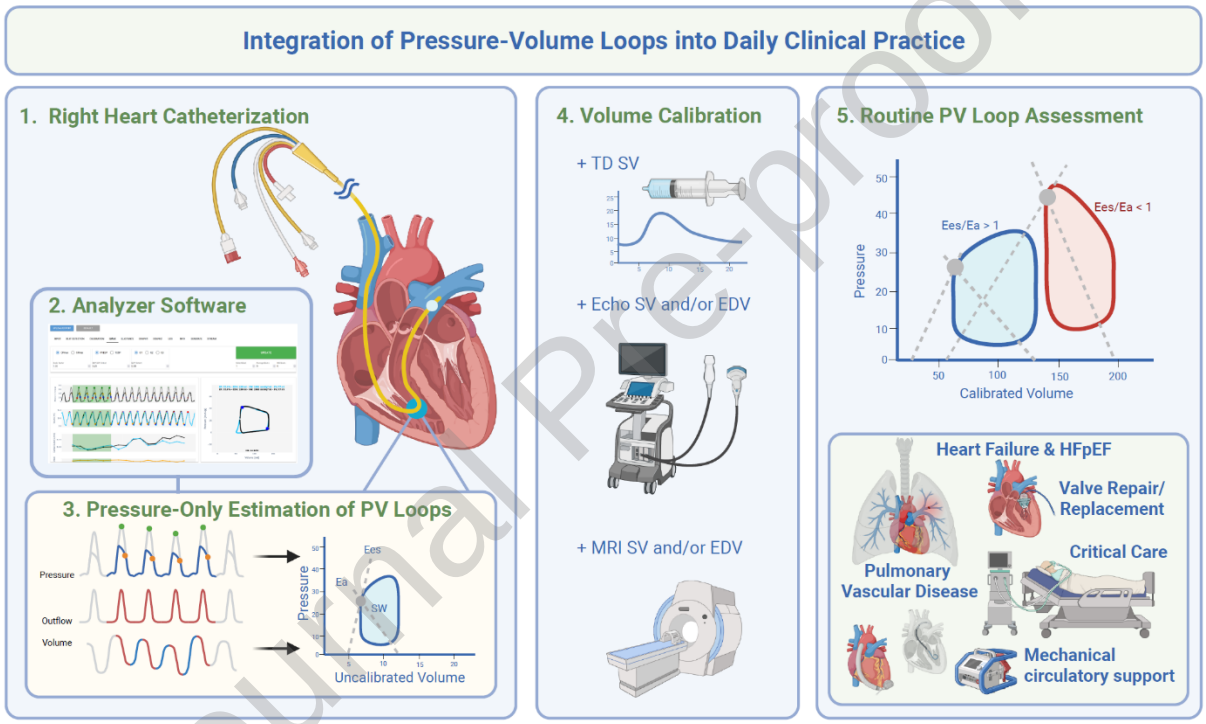

Graphical abstract Workflow and clinical integration of the novel method for deriving right ventricular pressure–volume (PV) loops from standard right heart catheterization (RHC) data.

Step 1: Sampling of pressure waveforms using a conventional Swan–Ganz catheter during routine RHC.

Step 2: Data processing by dedicated analyzer software.

Step 3: Reconstruction of volume and generation of uncalibrated PV loops with a pressure-only model.

Step 4: External volume calibration by using stroke volume (SV) or end-diastolic volume (EDV) estimates from thermodilution (TD), echocardiography, or cardiac magnetic resonance imaging (MRI).

Step 5: Derivation of absolute PV loops with quantitative coupling metrics, including end-systolic elastance (Ees), arterial elastance (Ea), stroke work (SW), and the Ees/Ea ratio. HFpEF, heart failure with preserved ejection fraction.

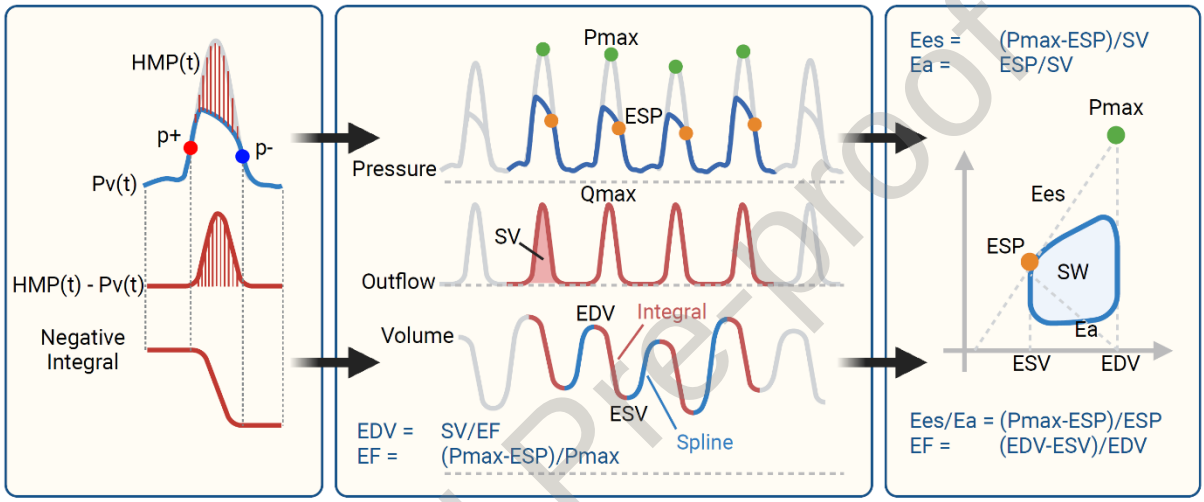

Figure 1 Graphical workflow of the pressure-only algorithm for reconstructing right ventricular pressure–volume loops. The uncalibrated flow curve is computed from the pressure gradient between HMP(t) and Pv(t), and is numerically integrated to generate the systolic portion of the volume curve. The diastolic volume phase is constructed via spline interpolation between the estimated ESV and EDV. The resulting volume curve, combined with the measured pressure waveform, is used to generate the final pressure–volume loop. The pressure points p+ (red) and p− (blue) correspond to the pressures at $dpdt_{max}$ and $dpdt_{min}$, respectively. Ea, arterial elastance; EDV, end-diastolic volume; Ees, end-systolic elastance; EF, ejection fraction; ESP, end-systolic pressure; ESV, end-systolic volume; HMP(t), hydromotive pressure waveform; P_{max}, theoretical peak pressure under isovolumic conditions; Pv(t), measured ventricular pressure; Q_{max}, peak flow; SV, stroke volume; SW, stroke work.

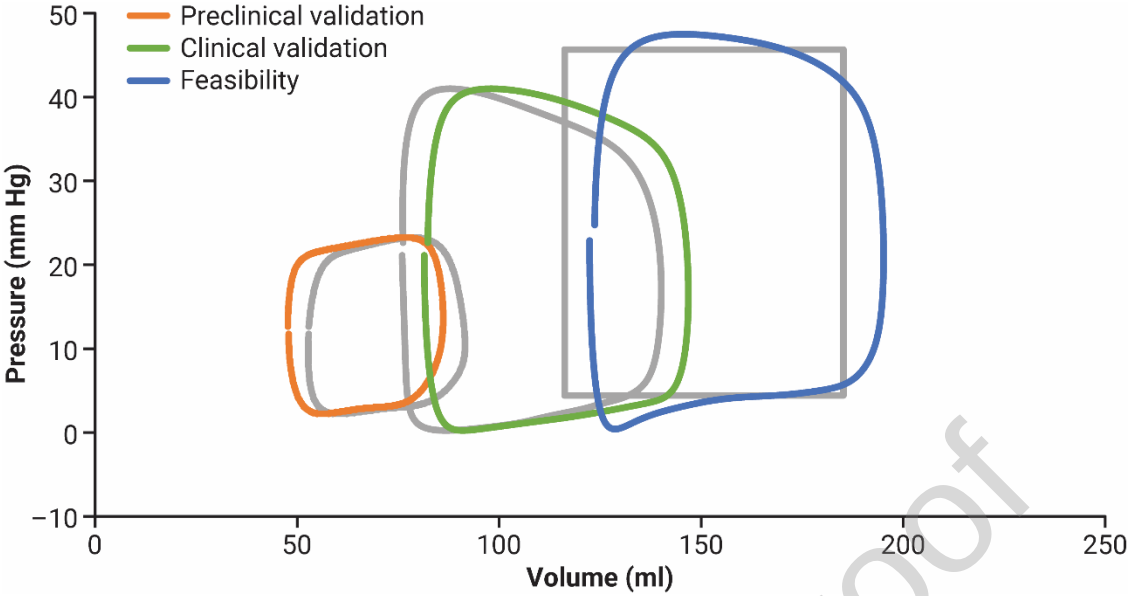

Figure 2 Mean pressure–volume loops generated using the pressure-only algorithm compared with reference loops. Reference loops (shown in grey) were obtained by conductance catheterization in the preclinical and clinical cohorts. In the feasibility cohort, algorithm-derived loops from standard RHC were calibrated against thermodilution and compared with 3-dimensional echocardiographic data as the reference. For graphical comparison of RHC and echocardiographic data, rectangular loops were constructed from the echocardiographic data using four corner points: 1. EDV, EDP; 2. EDV, ESP; 3. ESV, ESP; and 4. ESV, EDP. EDP, end-diastolic pressure; EDV, end-diastolic volume; ESP, end-systolic pressure; ESV, end-systolic volume.

Table 1 Comparative Regression and Bland–Altman Analysis

Cohort	Parameter	Reference	Regression	Bias	Limits of agreement	Percentage error
Preclinical (swine, *n* = 22)	SW, mm Hg·ml	CC*	r = 1.00, *p* < 0.001	−4.7 (−0.4%)	−56.5 to 47.1 (−8.1% to 7.4%)	7.0%
	EDV, ml	CC*	r = 0.82, *p* < 0.001	4.5 (3.7%)	−21.8 to 30.8 (−24.0% to 31.4%)	29.0%

Clinical (RV study cohort, *n* = 44)	SW, mm Hg·ml	CC (MRI)	r = 0.99, *p* < 0.001	−56.6 (−2.8%)	−364.6 to 251.4 (−17.5% to 11.9%)	14.6%
	EDV	CC (MRI)	r = 0.90, *p* < 0.001	−6.7 (−5.5%)	−55.3 to 41.8 (−38.5% to 27.5%)	35.3%
Feasibility (routine RHC, *n* = 29)	SV, ml	3DE	r = 0.79, *p* < 0.001	−0.5 (−1.0%)	−22.0 to 21.0 (−31.3% to 29.4%)	30.2%
	EDV, ml	3DE	r = 0.87, *p* < 0.001	−6.5 (−4.4%)	−55.4 to 42.4 (−32.2% to 23.4)	26.5%
	EF	3DE	r = 0.80, *p* < 0.001	0.01 (2.2%)	−0.11 to 0.14 (−31.1% to 35.4%)	30.3%
	Ees, mm Hg/ml	3DE	r = 0.94, *p* < 0.001	0.00 (−1.4%)	−0.15 to 0.14 (−33.3% to 30.5%)	34.8%
	Ea, mm Hg/ml	3DE	r = 0.96, *p* < 0.001	−0.02 (−1.4%)	−0.31 to 0.27 (−33.3% to 30.5%)	41.3%

3DE, 3-dimensional echocardiography; CC, conductance catheterization; Ea, arterial elastance; EDV, end-diastolic volume; Ees, end-systolic elastance; EF, ejection fraction; MRI, magnetic resonance imaging; RHC, right heart catheterization; RV, right ventricular; SV, stroke volume; SW, stroke work.

*Saline parallel conductance + flow probe

Table 2 *Population Data – Clinical Validation Cohort*

Variable	**Control (*n* = 15)**	**PAH/CTEPH (*n* = 22)**	**IpcPH (*n* = 7)**	**All (*n* = 44)**
Female, *n*	10	14	3	27

Age, years	58.0 (45.0–63.5)	57.0 (50.0–67.0)	77.0 (73.0–79.0)	61.0 (50.0–70.5)
Weight, kg	96.0 (75.0–105.0)	74.5 (66.0–82.3)	81.0 (72.0–92.0)	77.5 (71.5–96.0)
Height, cm	174.5 ± 9.0	167.9 ± 9.9	172.3 ± 7.9	170.8 ± 9.6
BSA, m^2	2.1 ± 0.2	1.8 ± 0.2	2.0 ± 0.2	1.9 ± 0.2
CO, l/min	5.7 ± 1.2	4.7 ± 1.1	5.3 ± 0.5	5.1 ± 1.2
CI, l/min/m^2	2.7 ± 0.5	2.5 ± 0.6	2.7 ± 0.3	2.6 ± 1.2
mPAP, mm Hg	17.0 (13.5–19.0)	34.5 (26.0–38.0)	35.0 (28.0–36.5)	26.0 (19.0–36.4)
PAWP, mm Hg	9.0 (7.0–10.5)	8.0 (7.0–9.8)	25.0 (18.0–25.0)	9.0 (7.0–11.3)
PVR, WU	1.6 (1.1–1.8)	5.3 (3.5–6.9)	2.0 (1.9–2.0)	2.4 (1.7–5.3)
mild TR, *n*	11	12	3	26
moderate TR, *n*	4	5	4	13
severe TR, *n*	0	5	0	5
EDV, ml	103.0 (81.5–116.0)	140.0 (134.3–176.5)	119.0 (108.0–151.0)	129 (107.3–154.3)
ESV, ml	42 (37.0–47.5)	78.0 (64.3–120.5)	68.0 (58.5–78.0)	64.0 (47.8–79.3)
SV, ml	57.6 ± 20.3	67.8 ± 13.4	55.3 ± 15.1	62.3 ± 16.9
SW, mm Hg·ml	1365.0 ± 515.2	2851.3 ± 1030.8	1633.7 ± 852.0	2108.6 ± 1075.9
ESP, mm Hg	16.6 (12.3–22.9)	45.7 (34.2–62.0)	49.2 (28.0–55.1)	35.1 (22.0–51.8)
P_{max}, mm Hg	40.7 (31.7–46.6)	70.9 (56.3–83.3)	75.5 (47.2–89.0)	58.5 (42.9–79.5)
EF	0.55 (0.52–0.59)	0.46 (0.37–0.51)	0.45 (0.40–0.48)	0.49 (0.44–0.54)
PBEF*	0.60 (0.46–0.65)	0.35 (0.30–0.41)	0.38 (0.33–0.47)	0.41 (0.32–0.49)

Data are presented as *n*, median (interquartile range), or mean ± standard deviation.

BSA, body surface area; CI, cardiac index; CO, cardiac output; CTEPH, chronic thromboembolic pulmonary hypertension; EDV, end-diastolic volume; EF, ejection fraction; ESP, end-systolic pressure; ESV, end-systolic volume; IpcPH, isolated postcapillary pulmonary hypertension; mPAP, mean pulmonary arterial pressure; PAH, pulmonary arterial hypertension; PAWP, pulmonary arterial wedge pressure; PBEF, pressure-based ejection fraction; P_{max}, theoretical peak pressure under isovolumic conditions; PVR, pulmonary vascular resistance; SV, stroke volume; SW, stroke work; TR, tricuspid regurgitation; WU, Wood Units.

*Calculated from $1-ESP/P_{max}$.

Table 3 *Population Data – Feasibility Cohort*

Variable	**Exclusion of PH (*n* = 8)**	**PH (Groups 1–5, *n* = 21)**	**All (*n* = 29)**
Female, *n*	2	11	13
Age, years	65.0 (48.0–70.3)	64.0 (47.0–74.0)	64.0 (47.0–74.0)
Weight, kg	84.0 (71.8–99.3)	79.0 (65.0–92.0)	82.0 (68.0–97.0)
Height, cm	177.3 ± 9.0	171.8 ± 11.5	173.3 ± 11.0
BSA, m²	2.0 ± 0.3	2.0 ± 0.3	2.0 ± 0.3
CO, l/min	6.4 ± 1.3	5.1 ± 1.7	5.5 ± 1.7
CI, l/min/m²	3.1 ± 0.7	2.6 ± 0.8	2.8 ± 0.8
mPAP, mm Hg	16.5 (15.8–18.3)	36.0 (27.0–49.0)	27.0 (23.0–42.0)
PAWP, mm Hg	8.0 (6.8–11.0)	8.0 (8.0–14.0)	8.0 (7.0–12.0)
PVR, WU	1.6 (1.3–1.6)	4.5 (3.2–9.0)	3.4 (1.6–5.5)
mild TR, *n*	7	8	15
moderate TR, *n*	1	9	10

severe TR, *n*	0	4	4
EDV, ml	166.2 (156.1–198.1)	180.8 (151.0–235.8)	174.0 (151.0–230.0)
ESV, ml	92.5 (70.2–118.4)	129.8 (85.0–162.6)	106.0 (76.4–138.0)
SV, ml	82.5 ± 18.6	67.2 ± 13.6	71.4 ± 16.4
ESP, mm Hg	21.5 (20.6–26.3)	53.3 (36.1–75.1)	37.9 (25.8–57.9)
P_{max}, mm Hg	43.9 (41.2–47.2)	75.0 (57.9–108.5)	65.2 (46.5–97.7)
EF	0.38 (0.30–0.45)	0.45 (0.40–0.51)	0.41 (0.31–0.48)
PBEF*	0.35 (0.30–0.41)	0.49 (0.43–0.52)	0.37 (0.31–0.46)

Data are presented as *n*, median (interquartile range), or mean ± standard deviation.

BSA, body surface area; CI, cardiac index; CO, cardiac output; EDV, end-diastolic volume; EF, ejection fraction; ESP, end-systolic pressure; ESV, end-systolic volume; mPAP, mean pulmonary arterial pressure; PAWP, pulmonary arterial wedge pressure; PBEF, pressure-based ejection fraction; PH, pulmonary hypertension; P_{max}, theoretical peak pressure under isovolumic conditions; PVR, pulmonary vascular resistance; SV, stroke volume; TR, tricuspid regurgitation; WU, Wood Units.

*Calculated from $1-ESP/P_{max}$.

Table 4 Comparison of 3D Echocardiography-derived with Algorithm-derived Parameters

Parameter	3D echocardiography	Calculated via thermodilution	*p*-value	ρ (Spearman)
EDV, ml	184.5 ± 48.2	191.0 ± 48.9	0.611	0.856 ($p < 0.001$)
ESV, ml	113.8 ± 44.1	119.1 ± 42.1	0.595	0.873 ($p < 0.001$)
SV, ml	71.4 ± 16.4	71.9 ± 17.7	0.911	0.852 ($p < 0.001$)

EF	0.40 ± 0.10	0.39 ± 0.09	0.569	0.785 ($p < 0.001$)
Ees, mm Hg/ml	0.40 (0.28–0.49)	0.41 (0.26–0.49)	0.920	0.923 ($p < 0.001$)
Ea, mm Hg/ml	0.71 (0.34–1.01)	0.73 (0.32–0.94)	0.846	0.965 ($p < 0.001$)

Data are presented as median (interquartile range) or mean ± standard deviation.

3D, 3-dimensional; Ea, arterial elastance; EDV, end-diastolic volume; Ees, end-systolic elastance; EF, ejection fraction; ESV, end-systolic volume; SV, stroke volume.